
Rank Reduction Autoencoders - Enhancing interpolation on nonlinear manifolds.

Jad Mounayer

ENSAM Institute of Technology
PIMM, SKF Chair
Blvd de l'Hôpital, Paris
jad.mounayer@outlook.com

Sebastian Rodriguez

ENSAM Institute of Technology
PIMM, RTE Chair
Blvd de l'Hôpital, Paris
sebastian.rodriguez_iturra@ensam.eu

Chady Ghnatios

ENSAM Institute of Technology
PIMM, SKF Chair
Blvd de l'Hôpital, Paris
chady.ghnatios@ensam.eu

Charbel Farhat

Department of Aeronautics and Astronautics,
Stanford University,
Stanford, 94305,
cfarhat@stanford.edu

Francisco Chinesta

ENSAM Institute of Technology
PIMM, ESI/Keysight Chair
CNRS@CREATE, Singapore
Blvd de l'Hôpital, Paris
francisco.chinesta@ensam.eu

Abstract

The efficiency of classical Autoencoders (AEs) is limited in many practical situations. When the latent space is reduced through autoencoders, feature extraction becomes possible. However, overfitting is a common issue, leading to “holes” in AEs’ interpolation capabilities. On the other hand, increasing the latent dimension results in a better approximation with fewer non-linearly coupled features (e.g., Koopman theory or kPCA), but it doesn’t necessarily lead to dimensionality reduction, which makes feature extraction problematic. As a result, interpolating using Autoencoders gets harder. In this work, we introduce the Rank Reduction Autoencoder (RRAE), an autoencoder with an enlarged latent space, which is constrained to have a small pre-specified number of dominant singular values (i.e., low-rank). The latent space of RRAEs is large enough to enable accurate predictions while enabling feature extraction. As a result, the proposed autoencoder features a minimal rank linear latent space. To achieve what’s proposed, two formulations are presented, a strong and a weak one, that build a reduced basis accurately representing the latent space. The first formulation consists of a truncated SVD in the latent space, while the second one adds a penalty term to the loss function. We show the efficiency of our formulations by using them for interpolation tasks and comparing the results to other autoencoders on both synthetic data and MNIST.

1 Introduction

Interpolation of vector functions over a parametric space is an active research topic since accurate interpolation allows the reconstruction of a physical solution in an entire parametric space from a set of pre-computed samples. Multiple techniques have been proposed to perform interpolation,

to mention a few, the Proper Orthogonal Decomposition with Interpolation (PODI) [24, 17, 19], or the sparse-PGD (sPGD) [7]. Most of these techniques are based on Model Order Reductions, such as the Proper Orthogonal Decomposition (POD) [12], the Proper Generalized Decomposition (PGD) [21, 6], and the Principal Component Analysis (PCA) [9]. These techniques stack the vector functions in what is called the solution matrix, and their efficiency is inversely proportional to the rank of this matrix. If the solution matrix only has a few dominant singular values (i.e., low-rank), it is easier for the aforementioned techniques to reduce the problem and interpolate. However, when this assumption does not apply, they fail to define an efficient surrogate for the correct prediction of physical phenomena. A high-rank solution matrix reduces the efficiency of techniques based on different formulations such as those based on Grassmann manifolds [1], the Optimal Transport (OT) [25], or every low-rank technique (e.g. [22, 14]).

On the other hand, the nonlinearity in autoencoders with Neural Networks as their encoding and decoding functions makes them appealing to be used as interpolators [10]. Their modified architectures have been used for different purposes in many applications such as speech recognition [4], biophysics [13], medicine [18], and others [2]. Yet, the efficiency of Vanilla Autoencoders is limited. On one hand, Autoencoders with reduced latent spaces (or Diabolo Autoencoders (DAEs)), can easily overfit the data and are known for having “holes” in their latent spaces. On the other hand, even though enlarged latent spaces lead to better approximations with less non-linear behavior (as stated in multiple theories like the Koopman theory or the kPCA), the representations learned are usually of a large dimension which limits both interpolation and feature extraction. This has led to multiple enhancements such as Variational AEs [8, 26], Sparse AEs [20], and denoising AEs [27] which improved Autoencoders overall but did not definitively solve the interpolation issues.

Neural Networks are increasingly being used for nonlinear reduction techniques [3, 5]. Recently, the Implicit Rank-Minimizing Autoencoder (IRMAE) [11], and the Low-Rank Autoencoder (LoRAE) [15] showcased how increasing the latent space dimension while encouraging a low-rank achieves better results, for both approximation and interpolation. If the latent space is of low rank, the efficiency of all presented interpolation techniques (including basic linear interpolation) in the latent space is enhanced. The resulting Autoencoder would benefit from the large data dimensionality of the latent space to find better approximations while allowing feature extraction because of its low rank. The architecture of IRMAEs consists of adding linear layers between the encoder and the latent space, while LoRAE only adds one linear layer as well as its nuclear norm as a penalty term in the loss. While both papers show how their resulting latent spaces may exhibit a lower rank compared to Vanilla and Variational Autoencoders, their work has some limitations. First, while both architectures may find a low-rank latent space with singular values that are sharply decreasing, they do not enforce the small singular values to go to zero. Accordingly, the decoder always has some noise from the small singular values, even though ideally, we would like to remove their effect entirely. In addition, the computational time of both architectures highly depends on the latent space dimension L . Since a long latent space usually helps in achieving better results, both IRMAEs and LoRAEs can be computationally expensive. Finally, both architectures do not provide explicit control over the rank of the latent space. While they include some tuning parameters, we show later in the paper that the optimal parameters proposed in [11, 15] can not reach a satisfying low-rank space.

In this paper, we present the Rank Reduction Autoencoder (RRAE), which has a large latent space restricted to have a low rank. By enforcing the latent space to accept a linear reduction (hence a lower rank), we show that our model resolves the issues previously mentioned. Our architecture includes two proposed formulations: (i) a strong and (ii) a weak one. Throughout the paper, we show that the strong formulation finds orthogonal basis vectors through a principal component analysis of the latent space, while the weak formulation is allowed to find non-orthogonal ones. Further, our results illustrate that both proposed formulations can interpolate efficiently whether between high-rank synthetic solutions, or between MNIST pictures while achieving both a lower latent space rank than the IRMAE and the LoRAE, and a lower computational overhead.

The present paper is structured as follows: Section 2 presents the architecture and both proposed formulations. Section 3 explains the insights behind long latent spaces with a low rank on two synthetic examples. Then, we compare the interpolation capabilities of RRAEs with IRMAEs, and LoRAEs on a variety of problems in section 4. We explain the limitations of the proposed formulations in section 5, before finally summarizing the main original contributions of the present paper in section 6.

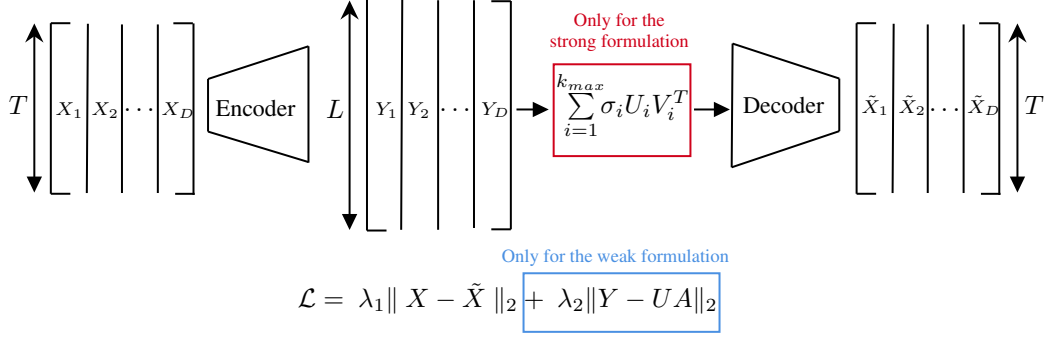


Figure 1: Schematic showing the autoencoder in use as well as both formulations. There are two terms in the loss function for the **weak formulation**. On the other hand, there's an additional step before the decoder for the **strong formulation**.

2 Rank Reduction Autoencoders (RRAEs)

To define the architecture of RRAEs, we begin by defining autoencoder notations. Let $\{X_i\}_{i \in [1, D]} \in \mathbb{R}^T$ be a set of D series of observations, each having T degrees of freedom. We define our input $X \in \mathbb{R}^{T \times D}$ with X_i as its i th column. Let, $Y \in \mathbb{R}^{L \times D}$, with L , the chosen dimension¹ of the latent space. We also define the encoding map $e : \mathbb{R}^{T \times D} \rightarrow \mathbb{R}^{L \times D}$ and the decoding map $d : \mathbb{R}^{L \times D} \rightarrow \mathbb{R}^{T \times D}$. The Vanilla autoencoder can be written as the following two operations,

$$Y = e(X), \quad \tilde{X} = d(Y). \quad (1)$$

In practice, we usually enforce that the output of the autoencoder gives us back the original data, hence the loss \mathcal{L} usually reads,

$$\mathcal{L}(X, \tilde{X}) = \|X - \tilde{X}\|_2, \quad \text{where, } \|\cdot\|_2 \text{ is the } L2\text{-norm.} \quad (2)$$

The idea behind RRAEs is to enforce the latent matrix to have a low rank while finding a reduced basis. In other words, if Y has a rank r , let $Y = U\Sigma V^T$ be the Singular Value Decomposition (SVD) [23, 16] of Y , with $U \in \mathbb{R}^{L \times r}$, $\Sigma \in \mathbb{R}^{r \times r}$, and $V^T \in \mathbb{R}^{r \times D}$. Let $\{\sigma_i\}_{i \in [1, r]}$ be the sorted diagonal values of Σ . Thus, by considering the k most significant modes (choice of k discussed in Section 4.2 and Appendix B), it results,

$$Y = \sum_{i=1}^r \sigma_i U_i V_i^T \quad \Rightarrow \quad Y \approx \sum_{i=1}^k \sigma_i U_i V_i^T, \quad k \ll r, \quad (3)$$

where U_i is the i th column of U and V_i^T is the i th row of V^T . In other words, we can write Y_d , the d th column of Y as,

$$Y_d \approx \sum_{i=1}^k (\sigma_i U_i V_i^T)_d = \sum_{i=1}^k \sigma_i U_i V_{i,d}^T = \sum_{i=1}^k \alpha_{i,d} U_i, \quad \forall d \in [1, D], \quad (4)$$

with $V_{i,d}^T$ being entry d of vector V_i^T .

Accordingly, for k modes, each column of Y is defined by k coefficients and k vectors. Further, vectors U_i form a basis for the latent space. We can write (4) in matrix form as follows,

$$Y \approx UA, \quad \text{with: } A_{i,j} = \alpha_{i,j}, \quad U \in \mathbb{R}^{L \times k}. \quad A \in \mathbb{R}^{k \times D}, \quad (5)$$

Based on (4), and (5), we propose two formulations that enforce the low rank of the latent space and find its reduced basis. The architecture is sketched in Figure 1.

1. **The weak formulation:** After choosing the maximum allowed number of modes k_{max} , we generate two trainable matrices $A \in \mathbb{R}^{k_{max} \times D}$, and $U \in \mathbb{R}^{L \times k_{max}}$. Afterward, we add a

¹See Appendix B for details on the choice of L .

term to the loss as seen in blue in Figure 1. By doing so, minimizing the loss means that the latent space would have at most a rank of k_{max} . After convergence, the columns of our trainable matrix U form the reduced basis of the latent space. Additionally, the coefficients found in matrix A describe how to reconstruct each column Y_d as a linear combination of the basis vectors. We will refer to this method as the weak formulation since throughout training, the Network minimizes a sum of both terms and not each term individually. Accordingly, predictions \tilde{X} could be less accurate, and we might end up with more modes than the specified value of k_{max} .

Remark: The two trainable matrices can be computed from a one-rank greedy procedure, as PGD performs.

2. **The strong formulation:** Unlike the weak formulation, this architecture enforces, in a strong manner, the maximum dimension of the reduced basis of the latent space. Similarly to the weak formulation, we begin by choosing the maximum rank k_{max} of the latent space. Then, as seen in red in Figure 1, a truncated SVD (of order k_{max}) of the latent space is given to the decoder, instead of the latent space itself. Accordingly, the input of the decoder (or our new latent space) will have at most k_{max} dominant singular values. We refer to this method as the strong formulation since we strictly enforce the latent space to have a rank that’s lower or equal to k_{max} . In this case, the basis vectors and coefficients are simply the ones found by the truncated SVD.

In both formulations, k_{max} is a hyperparameter to be chosen. We propose a strategy to choose this hyperparameter and discuss its effect in Section 4.2 and in Appendix B.

When using the strong formulation, we compute a POD basis, where the vectors are by construction orthogonal. The orthogonality of the basis vectors, as well as refraining from adding terms in the loss, can enhance both the training and interpolation results. On the other hand, backpropagation through the singular value decomposition is not common in practice. All the work presented in this paper was performed using `equinox` in `JAX`, where gradients of the singular value decomposition are implemented and accessible.

Both formulations reduce the limitations of IRMAE and LoRAE. We sum up our contributions as follows:

1. RRAEs with a strong formulation lead to low-rank latent spaces that have many singular values exactly equal to zero. In other words, the decoder will get a sum of exactly k_{max} rank-one updates. As will be shown later in the paper, this gives the strong formulation an advantage for training and interpolation.
2. The computational overhead of RRAEs is reduced compared to other architectures, especially for large latent spaces. For the strong formulation, when batches are used, the SVD is only performed on a matrix of size $L \times bs$, bs being the batch size. Similarly, for the weak formulation, the added computational cost is minimal since the trainable matrices are of shape $L \times k_{max}$ and $k_{max} \times D$ with $k_{max} \ll L$. On the other hand, the IRMAE or the LoRAE either performs a gradient descent or finds the nuclear norm of an $L \times L$ matrix. Since a large latent space dimension L usually helps in achieving better results, both IRMAEs and LoRAEs can be computationally challenging.
3. Both formulations give us explicit control over the rank of the latent space. Accordingly, RRAEs allow us to perform feature extraction while benefitting from the advantages of long latent spaces. Additionally, as shown next in the paper, we can enforce the latent space to have a lower rank than IRMAE and LoRAE, which leads to better interpolation.

3 Insights behind Long latent spaces with low rank

An enlarged latent space can exhibit a linear behavior (as explored for instance in the Koopman theory, or the kPCA). Furthermore, a latent space with a reduced basis allows easier interpolation and feature extraction. The Diabolo Autoencoder on the other hand has “holes” in its interpolation [11], since it does not find a basis, but only a set of coefficients that are helpful for the decoder to retrieve the solution. Since the decoder is highly nonlinear, these coefficients can be anything, which leads to overfitting.

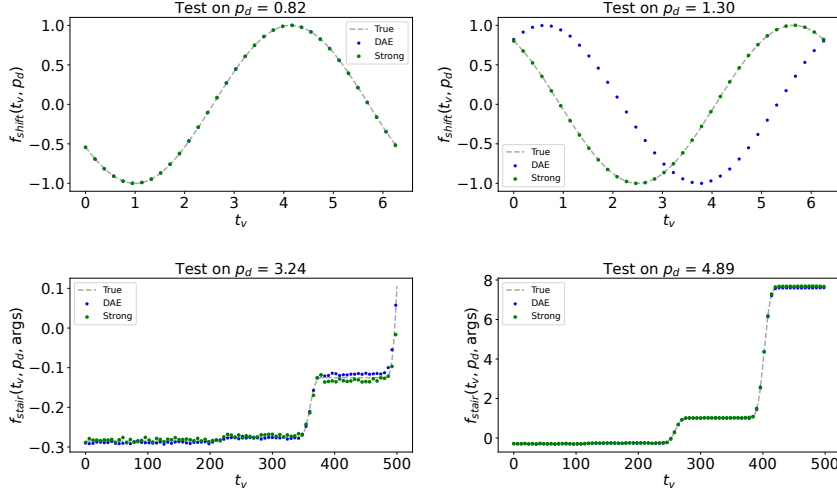


Figure 2: Predictions of DAEs and RRAEs with the strong formulation over two particular values of p_d for the shifted sine (above) and the stair-like examples (below).

To illustrate the aforementioned arguments, we test DEAs and our strong formulation on two examples characterized by one parameter. The first curves we propose are shifted sine curves since these have a simple nonlinearity, but they are hard to separate (nonmonotonic and cross each other multiple times). For our second example, we chose curves with stair-like behavior. In that case, we create highly nonlinear curves (different supports, different numbers of jumps of different magnitudes), but we define them to be monotonic and only cross each other occasionally (i.e. easier to separate). The equations used to define the columns of our input matrix X in each case are as follows,

$$\begin{cases} X_d(t_v, p_d) = f_{shift}(t_v, p_d) = \sin(t_v - p_d\pi), & p_d \in [0, 1.7], \\ X_d(t_v, p_d) = f_{stair}(t_v, p_d, args) & p_d \in [1, 5], \end{cases}$$

where $t_v \in \mathbb{R}^T$ is the time discretization vector, and f_{stair} takes some arguments “args” as detailed in the algorithm in Appendix A. The training is performed over 17, and 40 equidistant values of p_d for the shifted sine curves and the stair-like curves respectively. Later on, we interpolate the resulting curves in the latent space of the autoencoders on 80 and 300 random values of p_d , respectively, chosen inside the training domain. The large number of tests guarantees that the models are learning the dynamics and not just the training curves and some tests nearby. Since the solution curves depend on one parameter, we use a DAE with a single scalar latent space and an RRAE with a longer latent space of rank one. We then linearly interpolate in the latent space to predict the test set. The training parameters, including the dimension of the latent space, can be found in Appendix B. The relative error over all p_d values for both the train and test sets is summarized in Table 1. Further, for each example, the predictions over some selected test cases are plotted in Figure 2.

Table 1: Relative error (in %) for the DAE and RRAE with the strong formulation on both the train and test sets for both the examples of shifted sin curves and stair-like ones.

Model	Shifted sine		Stair-like	
	Train Error	Test error	Train Error	Test error
DAE	2.12	32.42	2.97	3.74
RRAE (strong)	1.73	1.90	1.87	3.2

The results show that when curves are hard to separate, RRAEs are better interpolators than DAEs. On the other hand, the effect of longer latent spaces is reduced for simple curves that can be highly nonlinear, but characterized by one parameter, and easily separable.

To further investigate the results, we plot the coefficients to be interpolated in the latent space as a function of the corresponding parameter p_d in Figure 3. It is important to note that the coefficients are

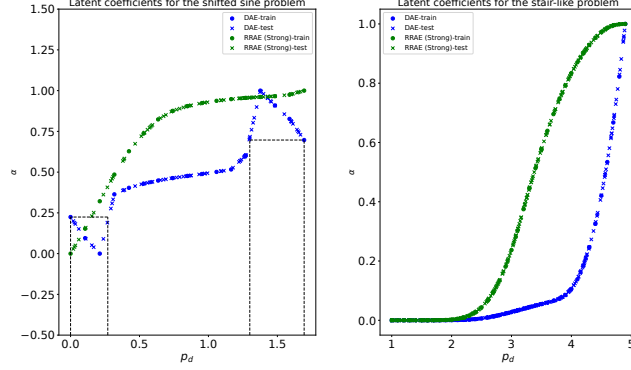


Figure 3: Normalized latent coefficients to be interpolated (dots) for DAE and RRAE with a strong formulation, and the interpolated values for the test set (crosses) for the shifted sine curves (left) and the stair-like curves (right).

defined differently between the RRAE and the DAE. For RRAEs, when $k_{max} = 1$, the coefficients are simply the entries of $A \in \mathbb{R}^{1 \times D}$ in equation (5). On the other hand, for a Diabolo Autoencoder with a scalar latent space, the values in the latent space themselves are the coefficients.

The main problem with the coefficients found by the DAE for the shifted sine curves (the blue crosses and dots in Figure 3 (left)) is that the resulting curve from linearly interpolating the coefficients is not an injection, over two significant parts of the domain. Specifically, for any value of p_d in approximately $[0, 0.3]$ and $[1.3, 1.5]$ (between the dotted lines), there exists another value with the same coefficient α , leading to the same decoded curve. Accordingly, the decoder will find the same curve for two different parameters, which is wrong since p_d defines a shift. This explains why the DAE can interpolate well in the top left subplot in Figure 2, but not in the top right one. These results also show what is meant by “holes” in the latent space for DAEs.

On the other hand, as proposed earlier, a longer latent space allows us to find better features. This is clearly shown by the coefficients of the strong formulation in Figure 3 (left), which have a monotonic behavior.

Finally, the right part of Figure 3 depicts that when the curves are simple to separate and are characterized by only one parameter, both architectures can find monotonic coefficients that fit both the train and test sets.

4 Testing on Numerical Data

The solutions interpolated in the previous section were only characterized by one parameter. In this section, we test RRAEs and compare them to IRMAEs, and LoRAEs on two examples with a parametric space of dimension two, as well as on the MNIST dataset. Throughout the paper, we don’t compare RRAEs with different variations of VAEs. Our future work will include a Variational version of RRAEs and its comparison to different VAE architectures.

4.1 Examples with two parameters

We generated two challenging synthetic tests for interpolation. First, we propose the sum of two sine curves with different frequencies, as well as two Gaussian bumps in two different locations. We show how in such examples both our formulations result in latent spaces with a lower rank and better results than IRMAEs and LoRAEs for the hyperparameters chosen (again, training details can be found in Appendix B). We define the columns of our input matrix $X_d(t_v, p_d) = f_{prob}$ for each problem as follows,

$$\begin{cases} f_{freqs}(t_v, \mathbf{p}_d) = \sin(p_d^1 \pi t_v) + \sin(p_d^2 \pi t_v), & p_d^1 \in [0.3, 0.5], \quad p_d^2 \in [0.8, 1], \\ f_{gauss}(t_v, \mathbf{p}_d) = 1.3e^{-\frac{(t_v - p_d^1)^2}{0.08}} + 1.3e^{-\frac{(t_v - p_d^2)^2}{0.08}}, & p_d^1 \in [1, 3], \quad p_d^2 \in [4, 6]. \end{cases}$$

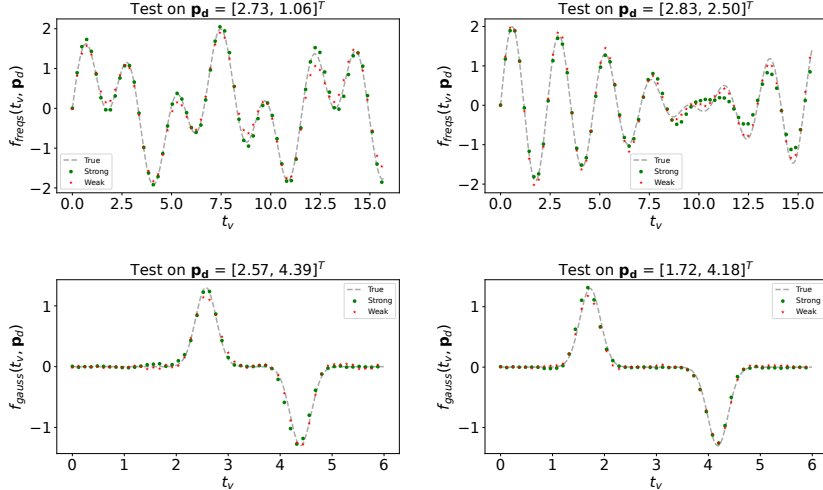


Figure 4: Interpolated results of RRAEs with both formulations on both examples presented with bilinear interpolation in the latent space.

We distinguish between the **bold** notation for vectors and non-bold ones for scalars. In both expressions, our parametric space is of dimension 2 and so $\mathbf{p}_d = [p_d^1, p_d^2]^T$. For each example and each architecture, we present some interpolated predictions in Figure 4, and the error over all the training/testing sets, as well as the average training time for 100 batches, are summarized in Table 2.

Table 2: Relative error (in %) for all architectures on both the train and test set for the two examples presented, and the average time (in s) for 100 batches (size 20).

Model	Two sines (freqs)		Two Gaussians		Average time
	Train Error	Test error	Train Error	Test error	
RRAE (strong)	6.33	12.83	4.46	8.75	1.61
RRAE (weak)	10.33	15.09	8.50	10.69	0.52
IRMAE (l=2)	6.95	17.35	4.68	13.93	3.6
IRMAE (l=4)	N/A	N/A	8.41	14.78	7.50
LoRAE	5.40	13.83	3.03	9.39	420.4

As can be seen in Table 2, RRAEs with the strong formulation are the most efficient in interpolation. Additionally, we note that increasing the parameter l for the IRMAE leads to divergence of the gradient descent in one of the problems (hence the N/A). Note that we only used the parameters specified in both papers for IRMAE and LoRAE. A fine-tuning of the parameters may potentially lead to better results for these architectures, but this venue is not investigated in this work. On the other hand, the table shows that RRAEs are faster than both IRMAEs and LoRAEs for the latent space dimension chosen. Our formulations are fast since we only add small matrices to the loss in the weak formulation, and we compute an SVD of an $L \times bs$ matrix, bs being the batch size, in the strong formulation. On the other hand, IRMAEs and LoRAEs find the gradient/the nuclear norm of an $L \times L$ matrix respectively, with L relatively large.

Additionally, we draw some of the normalized singular values of the latent space for the problem with the two Gaussians in Figure 5. The figure illustrates that adding the number of linear layers for the IRMAE (i.e. increasing l) indeed reduces the rank of the latent space. However, both of our formulations can be restricted to finding latent spaces with lower ranks. In addition, it is important to note that even though the LoRAE has a low error overall, the latent space rank is still relatively high compared to the other techniques (as can be seen from the slowly decreasing singular values in violet in Figure 5 (left)). Hence, the trained model can not efficiently be used for other tasks, such as feature extraction. From the log-scaled graph illustrated in Figure 5 (right), we can understand why the strong formulation achieves the best results. As previously mentioned, the IRMAE, the LoRAE and our weak formulation don't enforce the singular values to fall to zero. So even though many

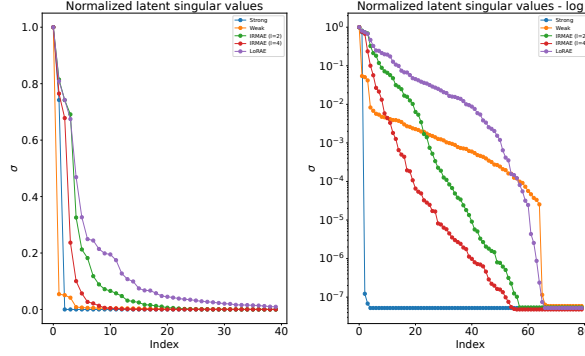


Figure 5: Normalized singular values of the latent space Y when trained over the two Gaussians. The first 40 singular values are shown to the left, and the first 80 singular values are shown on a log scale to the right.

singular values are small, they still have a noise effect over the decoder, which reduces their efficiency in interpolation.

4.2 Testing on MNIST

In this section, we compare our architecture to the IRMAE and the LoRAE on the MNIST dataset. Previously on our synthetic data, we showed that interpolating between two sine curves (for instance), in the latent space leads to another decoded sine function (and not a random one). Similarly, autoencoders should be able to interpolate between MNIST pictures of numbers to find other pictures of numbers in between. To illustrate this, we begin by training an autoencoder with each architecture on all 60,000 pictures from the training set (training parameters are available in Appendix B). Then, we use each model to create interpolated pictures and form an “interpolated set”. Interpolation is done by randomly choosing two pictures from the training set (e.g., leftmost and rightmost in Figure 6) and linearly interpolating their latent variables to find five new pictures in between. Interpolated pictures (in the red rectangle from left to right in Figure 6) are expected to transition from the leftmost picture to the rightmost one in an equidistant manner. For instance, the latent coefficients for the pictures in the second column of subplots in Figure 6 take $5/6$ of the latent coefficients of the first picture (i.e. number 7) and $1/6$ of those of the last picture (i.e. number 3). Similarly, latent variables for pictures in the third column would have proportions of $4/6$ and $2/6$ respectively. This procedure is then repeated 2000 times to create, for each architecture, an interpolated set of size 10,000. To quantify the quality of the generated images, we train a classifier on the original training set and test

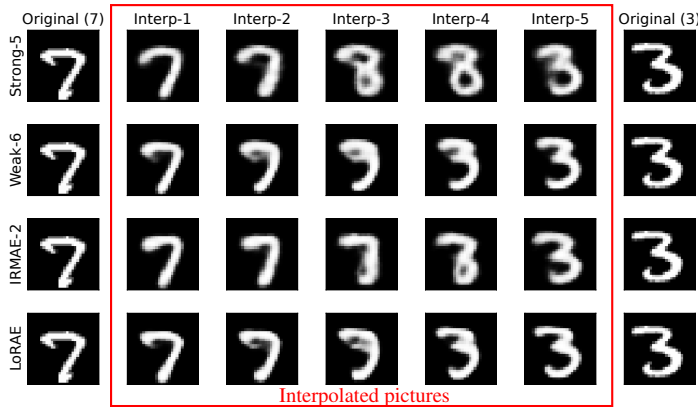


Figure 6: Five-step interpolation between a number 7 (leftmost) and a number 3 (rightmost) on MNIST using RRAEs with both formulations, IRMAEs, and LoAREs. Numbers next to method names represent k_{max} for the RRAEs and the number of linear layers l for the IRMAE.

it on the interpolated set generated by each architecture. Our classifier is a multilayer perceptron with a softmax final activation function (details in Appendix B). It takes as input an MNIST picture and outputs a probability for every possible class (i.e., in $[0, 1]^{10}$). Since the labels of the interpolated images are unknown, we measure the success of classification by the certainty of the classifier, which we quantify by the entropy of the probability distribution written as follows,

$$H = \frac{-1}{10000} \sum_{i=1}^{10000} \sum_{j=1}^{10} p_j^i \log(p_j^i), \quad (6)$$

with p_j^i being the probability of class j predicted by the softmax activation function for sample i . More details about the entropy can be found in Appendix E. The lower the entropy, the more the classifier is certain about the class prediction of the interpolated image. Hence a low entropy means that the interpolated images resemble numbers between 0 and 9, just like the original dataset. We perform training using our strong formulation with three choices of k_{max} to illustrate how the choice of this hyperparameter affects the model. We also generate five different interpolated sets for each architecture using different training images for interpolation. The mean and standard deviation of the entropy over the five sets are presented in Table 3.

Table 3: Mean entropy, standard deviation (over five different interpolation sets) and the rank of the latent space for the strong formulation with three values of k_{max} , the weak formulation with $k_{max} = 6$, the IRMAE with $l = 2$, and the LoRAE, on their corresponding MNIST interpolated sets.

Model	Strong-3	Strong-5	Strong-8	Weak-6	IRMAE-2	LoRAE
H	$0.59 \pm 3e-3$	$0.5 \pm 2e-3$	$0.5 \pm 6e-3$	$0.53 \pm 5e-3$	$0.53 \pm 4e-3$	$0.51 \pm 6e-3$
Rank	3	5	8	6	8	20

The table illustrates how the choice of k_{max} can be made. We propose to start with a small value and increase it until the error stagnates. In this case, $k_{max} = 5$ seems to be a good choice. Both Table 3 and Figure 6 illustrate how RRAEs can interpolate well between MNIST pictures while using a lower rank. The strong formulation, for instance, recognizes that it is hard to go from 7 to 3 and goes through 8 (first line interp-3,4,5 in figure 6), while the others find unclear figures along the way. Further, while the LoRAE has a low entropy, its latent space has 20 dominant singular values, which doesn't allow any feature extraction. On the other hand, compared to IRMAEs in Table 3, the noise from the smaller singular values as well as the explicit control over the rank allows us to get a lower entropy while using a lower rank for the strong formulation (Strong-5). Further, we can observe that the weak formulation can achieve similar results to the IRMAE with a lower rank (6 compared to 8).

5 Limitations

As illustrated in the paper's results, RRAEs with both formulations can interpolate well while using a latent space with a lower rank. However, our proposed model has some limitations:

1. Even though both of our formulations allow explicit control over the rank of the latent space, k_{max} is a hyperparameter to be tuned. In practice, starting with a small value of k_{max} and increasing it until error convergence is a good strategy. In general, other techniques (e.g., PCA) could be used to approximate the intrinsic dimension of the latent space "à priori".
2. The weak formulation adds regularisation constants to the loss, which can be hard to tune. In practice, we had to repeat training multiple times to tune the parameters, which isn't ideal, especially for a larger dataset such as the MNIST.
3. For high dimensional problems with very long latent spaces, the strong formulation can be computationally expensive. Even though the SVD is only performed on a matrix of size $L \times bs$, bs being the batch size and L the length of the latent space, the cost of computing an SVD and backpropagating through it when L is excessively large can be high.
4. The effect of a long latent space is reduced when the solution is simple and separable. In such cases, an increased dimension of the latent space, hence RRAEs, may not be necessary.

6 Summary and Conclusions

In this article, we presented Rank Reduction Autoencoders (RRAEs), Autoencoders with latent spaces that accept linear reduction. We proposed two formulations, a weak and a strong one to find the latent space while building its reduced basis. Even though the basis vectors in the strong formulation are orthogonal, and they need not be in the weak formulation, we showed that both formulations can interpolate correctly between curves. Overall, our results show that the strong formulation has a superior capability of interpolation since it doesn't have any noise from small nonzero singular values in the latent space. We also showed that both the strong and the weak formulations can achieve lower and controlled ranks in the latent space. Accordingly, they can be used for feature extraction and can interpolate better. Finally, both formulations are fast to train, with the weak formulation being the fastest. While the strong formulation leads to better predictions, the weak formulation is much simpler to implement since it only adds a penalty term to the loss.

References

- [1] David Amsallem and Charbel Farhat. Interpolation method for adapting reduced-order models and application to aeroelasticity. *Aiaa Journal - AIAA J*, 46:1803–1813, 07 2008. doi: 10.2514/1.35374.
- [2] Dor Bank, Noam Koenigstein, and Raja Giryes. Autoencoders. *Machine learning for data science handbook: data mining and knowledge discovery handbook*, pages 353–374, 2023.
- [3] Joshua L Barnett, Charbel Farhat, and Yvon Maday. Neural-network-augmented projection-based model order reduction for mitigating the kolmogorov barrier to reducibility of cfd models, 2022.
- [4] Sarath Chandar A P, Stanislas Lauly, Hugo Larochelle, Mitesh Khapra, Balaraman Ravindran, Vikas C Raykar, and Amrita Saha. An autoencoder approach to learning bilingual word representations. In Z. Ghahramani, M. Welling, C. Cortes, N. Lawrence, and K.Q. Weinberger, editors, *Advances in Neural Information Processing Systems*, volume 27. Curran Associates, Inc., 2014. URL https://proceedings.neurips.cc/paper_files/paper/2014/file/2bcab9d935d219641434683dd9d18a03-Paper.pdf.
- [5] Yingyi Chen, Qinghua Tao, Francesco Tonin, and Johan Suykens. Primal-attention: Self-attention through asymmetric kernel svd in primal representation. In A. Oh, T. Nauermann, A. Globerson, K. Saenko, M. Hardt, and S. Levine, editors, *Advances in Neural Information Processing Systems*, volume 36, pages 65088–65101. Curran Associates, Inc., 2023. URL https://proceedings.neurips.cc/paper_files/paper/2023/file/cd687a58a13b673eea3fc1b2e4944cf7-Paper-Conference.pdf.
- [6] Francisco Chinesta and Elias Cueto. *PGD-based modeling of materials, structures and processes*. Springer, Switzerland, 2014.
- [7] Francisco Chinesta, Pierre Ladeveze, and Elias Cueto. A short review on model order reduction based on proper generalized decomposition. *Archives of Computational Methods in Engineering*, 18(4):395–404, 2011.
- [8] Eizaburo Doi and Michael Lewicki. Sparse coding of natural images using an over-complete set of limited capacity units. In L. Saul, Y. Weiss, and L. Bottou, editors, *Advances in Neural Information Processing Systems*, volume 17. MIT Press, 2004. URL https://proceedings.neurips.cc/paper_files/paper/2004/file/309a8e73b2cdb95fc1affa8845504e87-Paper.pdf.
- [9] David González, José Vicente Aguado, E Cueto, E Abisset-Chavanne, and F Chinesta. kpcabased parametric solutions within the pgd framework. *Archives of Computational Methods in Engineering*, 25:69–86, 2018.
- [10] Guillaume Hugué, Daniel Sumner Magruder, Alexander Tong, Oluwadamilola Fasina, Manik Kuchroo, Guy Wolf, and Smita Krishnaswamy. Manifold interpolating optimal-transport flows for trajectory inference. In S. Koyejo, S. Mohamed, A. Agarwal, D. Belgrave, K. Cho, and A. Oh, editors, *Advances in Neural Information Processing Systems*, volume 35, pages 29705–29718. Curran Associates, Inc., 2022. URL https://proceedings.neurips.cc/paper_files/paper/2022/file/bfc03f077688d8885c0a9389d77616d0-Paper-Conference.pdf.
- [11] Li Jing, Jure Zbontar, and yann lecun. Implicit rank-minimizing autoencoder. In H. Larochelle, M. Ranzato, R. Hadsell, M.F. Balcan, and H. Lin, editors, *Advances in Neural Information Processing Systems*, volume 33, pages 14736–14746. Curran Associates, Inc., 2020. URL https://proceedings.neurips.cc/paper_files/paper/2020/file/a9078e8653368c9c291ae2f8b74012e7-Paper.pdf.
- [12] Gaetan Kerschen, Jean-claude Golinval, Alexander F Vakakis, and Lawrence A Bergman. The method of proper orthogonal decomposition for dynamical characterization and order reduction of mechanical systems: an overview. *Nonlinear dynamics*, 41:147–169, 2005.
- [13] Tianxiao Li, Hongyu Guo, Filippo Grazioli, Mark Gerstein, and Martin Renqiang Min. Disentangled wasserstein autoencoder for t-cell receptor engineering. In A. Oh, T. Nauermann, A. Globerson, K. Saenko, M. Hardt, and S. Levine, editors, *Advances in Neural Information Processing Systems*, volume 36, pages 73604–73632. Curran Associates, Inc., 2023. URL https://proceedings.neurips.cc/paper_files/paper/2023/file/e95da8078ec8389533c802e368da5298-Paper-Conference.pdf.

- [14] Guangcan Liu, Zhouchen Lin, Shuicheng Yan, Ju Sun, Yong Yu, and Yi Ma. Robust recovery of subspace structures by low-rank representation. *IEEE transactions on pattern analysis and machine intelligence*, 35(1):171–184, 2012.
- [15] Alokendu Mazumder, Tirthajit Baruah, Bhartendu Kumar, Rishab Sharma, Vishwajeet Pattanaik, and Punit Rathore. Learning low-rank latent spaces with simple deterministic autoencoder: Theoretical and empirical insights, 2023.
- [16] Yuji Nakatsukasa. Accuracy of singular vectors obtained by projection-based svd methods. *BIT Numerical Mathematics*, 57(4):1137–1152, 2017.
- [17] Minh-Nhan Nguyen and Hyun-Gyu Kim. An efficient podi method for real-time simulation of indenter contact problems using rbf interpolation and contact domain decomposition. *Computer Methods in Applied Mechanics and Engineering*, 388:114215, 2022.
- [18] Daehyung Park, Yuuna Hoshi, and Charles C Kemp. A multimodal anomaly detector for robot-assisted feeding using an lstm-based variational autoencoder. *IEEE Robotics and Automation Letters*, 3(3):1544–1551, 2018.
- [19] RR Rama and S Skatulla. Towards real-time modelling of passive and active behaviour of the human heart using podi-based model reduction. *Computers & Structures*, 232:105897, 2020.
- [20] Marc' aurelio Ranzato, Y-lan Boureau, and Yann Cun. Sparse feature learning for deep belief networks. In J. Platt, D. Koller, Y. Singer, and S. Roweis, editors, *Advances in Neural Information Processing Systems*, volume 20. Curran Associates, Inc., 2007. URL https://proceedings.neurips.cc/paper_files/paper/2007/file/c60d060b946d6dd6145dcbad5c4ccf6f-Paper.pdf.
- [21] S Rodriguez, David Néron, P-E Charbonnel, Pierre Ladevèze, and G Nahas. Non incremental latin-pgd solver for non-linear vibratory dynamics problems. In *14ème Colloque National en Calcul des Structures, CSMA 2019*, 2019.
- [22] Nathan Srebro and Tommi Jaakkola. Weighted low-rank approximations. In *Proceedings of the 20th international conference on machine learning (ICML-03)*, pages 720–727, 2003.
- [23] Gilbert W Stewart. On the early history of the singular value decomposition. *SIAM review*, 35(4):551–566, 1993.
- [24] Marco Tezzele, Nicola Demo, and Gianluigi Rozza. Shape optimization through proper orthogonal decomposition with interpolation and dynamic mode decomposition enhanced by active subspaces, 2019.
- [25] Sergio Torregrosa, Victor Champaney, Amine Ammar, Vincent Herbert, and Francisco Chinesta. Hybrid twins based on optimal transport. *Computers & Mathematics with Applications*, 127: 12–24, 2022. ISSN 0898-1221. doi: <https://doi.org/10.1016/j.camwa.2022.09.026>. URL <https://www.sciencedirect.com/science/article/pii/S0898122122004060>.
- [26] Aaron van den Oord, Oriol Vinyals, and koray kavukcuoglu. Neural discrete representation learning. In I. Guyon, U. Von Luxburg, S. Bengio, H. Wallach, R. Fergus, S. Vishwanathan, and R. Garnett, editors, *Advances in Neural Information Processing Systems*, volume 30. Curran Associates, Inc., 2017. URL https://proceedings.neurips.cc/paper_files/paper/2017/file/7a98af17e63a0ac09ce2e96d03992fbc-Paper.pdf.
- [27] Pascal Vincent, Hugo Larochelle, Yoshua Bengio, and Pierre-Antoine Manzagol. Extracting and composing robust features with denoising autoencoders. In *Proceedings of the 25th international conference on Machine learning*, pages 1096–1103, 2008.

Appendix A Algorithm for the stair-like function

Algorithm 1: Algorithm to find f_{stair} for a parameter p_d .

Input: $p_d \in \mathbb{R}, t_v \in \mathbb{R}^T, (\text{Ph}_0, \text{Amp}_0, \kappa, y_0, w) \in \mathbb{R}$

$$\text{Amp}_{p_d} = p_d$$

$$\text{Ph}_{p_d} = \text{Ph}_0 + \kappa(\text{Amp}_{p_d} - \text{Amp}_0)$$

$$g_{p_d}(t_v) = \text{Amp}_{p_d} \sqrt{t_v} \sin(w(t_v - \text{Ph}_{p_d})) - y_0$$

$$h_{p_d}(t) = \left(\frac{|g_{p_d}(t)| + g_{p_d}(t)}{2} \right)^5$$

$$X_d(t_v, p_d) = \text{cumsum}(h_{p_d}(t_v))$$

Output: $X_d(t_v, p_d)$ for each parameter p_d .

In this paper, we choose the initial parameters of the stair function to be,

$$\begin{cases} \text{Ph}_0 = 0.875, & \text{Amp}_0 = 1 \\ \kappa = 2.286, & y_0 = 2.3, & w = 2\pi. \end{cases}$$

Appendix B Training details

The main purpose of this appendix is to allow readers to reproduce the results, and share the parameters we used to train the models.

B.1 Hyperparameters for synthetic data and PC properties

In general, the main parameters for RRAEs are the dimension of the latent space, k_{max} , the encoder/decoder architectures, learning rates, epochs, and batch sizes. For each problem, we fix the common parameters between all architectures. We try to only change necessary parameters between different examples, to show that training RRAEs, especially with the strong formulation, doesn't require too much hyperparameters tuning. For all problems (except MNIST) and all formulations, we use an encoder of depth 1 and width 64, and a decoder of depth 6 and width 64. Additionally, we use batches of size 20, the `softplus` as activation function between all layers, and the `adabelief` optimizer. Furthermore, we use multiple learning rates, starting with $1e-3$ and dividing by 10 until reaching $1e-5$ (3 steps). In each step, we train for 2000 batches. however, we impose stagnation criteria which usually stop training earlier. Further, we normalize the data by subtracting the mean and dividing by the standard deviation. We found that normalization was necessary, especially for the stair-like functions.

Throughout the paper, the only two parameters that we vary for RRAEs are the length of the latent space L and a coefficient κ_w that changes the learning rates for the trainable matrices of the weak method. In practice, we found that changing the learning rate of the trainable matrix A for the weak formulation is easier than changing the weights in the loss. Accordingly, while we use the same learning rate strategy proposed before for the encoder/decoder, we propose to multiply the learning rate by a constant κ_w before applying it to the trainable matrix A . By doing so, we find that there is no need to tune the loss parameters (i.e. both are equal to one). It is important to note that the vectors in the trainable matrix U are normalized at every training step so A captures the coefficients. In Table 4, we illustrate the latent space dimension L and the constant κ_w used for all the illustrated examples in this work (N/A means the weak method was not used for this example).

Next, we detail how the choice of k_{max} was made for each example. In general, an approximation of k_{max} can be found using multiple techniques (e.g. PCA). However, in this paper, we chose a simpler approach. If this hyperparameter is too small, the model will not converge, but if it is too large, the Neural Network will simply learn a latent space of a higher rank. Accordingly, we started with a

Table 4: Different values of the latent space length L and the constant κ_w that are used for all the examples in this work (except MNIST).

Param.	Shifts	Stair-like	Mult. Freqs.	Mult. Gauss.
L	4500	4500	2800	2800
κ_w	N/A	N/A	0.66	0.13

small value of k_{max} and increased it until the error converged. The values chosen for each example are detailed in Table 5.

Table 5: Different values of k_{max} that are used for all the examples in this work (except MNIST).

Param.	Shifts	Stair-like	Mult. Freqs.	Mult. Gauss.
k_{max}	1	1	12	2

As can be seen in the table, while we were able to choose exactly the dimension of the parametric space for most of the examples, for the sine curves with different frequencies, the method needed a higher rank in the latent space to converge to the low errors presented. This is mainly because the latent space was not long enough for the problem. However, we tried to fix the parameter L , so we had to change k_{max} accordingly. On the other hand, we chose the parameters that were shown to give the best results for the IRMAE and the LoRAE. We tried to have two and four linear layers for the IRMAE (i.e. $l = 2$ and $l = 4$), and we used a weight of 0.001 in the loss for the LoRAE (the optimal value specified in the presenting paper). Other parameter values for LoRAE and IRMAE were tested with little improvements overall. However, a fine-tuned choice of parameters could lead to better results than the ones presented in the paper. To ensure a fair comparison, every other parameter of these models was chosen to be the same as RRAEs (the ones listed before).

Since we provide average computational times in Section 4.1, we give some details about the machine used to generate these results. The PC used is an MSI Stealth 17Studio A13VH. The processor is Intel (13th generation), Core i9, 2600 MHz, 14 CPUs. The PC also has 64 GB of RAM. The library used was `equinox`, in JAX for the training. However, the code was only run on CPUs.

B.2 Hyperparameters for MNIST

The architecture for the MNIST dataset was different since convolutional Neural Networks were used. We fixed the kernel size to 4, the padding to 1, and the stride to 2 for each convolution/convolution transpose. For the encoder, we used convolutions with output 32, 64, 128, and 256 respectively, with relu activation functions in between. These were followed by a flattening layer, and a Multilayer Perceptron (MLP) with softplus activation functions, of depth 2, and width 64. The output of the MLP was fixed to be 128, the dimension of the latent space. On the other hand, the decoder included an MLP with depth 2, width 64, and softplus activation functions with an output dimension of 1568. The vector was then reshaped into a tensor of shape (32, 7, 7), which was then followed by two transposed convolutions with output shapes 8, and 1 respectively. For training, we used a learning rate of 0.0001, the optimizer `adabelief`, and a total of 50 epochs.

Even though the architecture and training are probably not the best ones, our purpose was to show that for a fixed architecture, RRAEs can outperform other existing methods and not achieve SOTA results over the MNIST since this was done for many architectures before.

While the choice of the hyperparameter k_{max} and l (for IRMAE) has been mentioned in Section 4.2, we used again the optimal weight in the loss proposed in the paper of LoRAE as $\lambda = 0.001$. We also used a factor $\kappa_w = 0.8$ for the weak formulation of RRAEs.

Now, we detail how our interpolation sets were created. As previously mentioned in the paper, we choose two random figures from the training set and generate five pictures by interpolating the latent space. This procedure is done 2000 times to generate the interpolation set. The entire thing is done 5 times to provide statistically significant results (i.e. with a mean and a standard deviation). For readers who would like to reproduce our results, we used the seeds 0, 10, 100, 1000, and 10000 to generate a `jax.random` key respectively. The key was then split into 2000 other keys (by using

`jax.random.split`). Finally, we fed these keys to create 2000 permutations of the indices of the training figures (i.e. 0 until 60,000) and only took the first two numbers as our choice of the figures to be interpolated. By using these seeds, readers should be able to exactly generate the interpolation sets used in the paper. In addition, the example presented in Figure 6 is the interpolation between pictures of indices 52 and 12.

B.3 Choice of parameters for synthetic data

Throughout the paper, we mentioned the range in which the values of \mathbf{p}_d were chosen for each example. In this subsection, we provide some details on the chosen values of \mathbf{p}_d , mainly to show that the test covers most of the parametric space. Throughout the paper, we presented curves with parametric spaces of one and two. The following figures show the plot of the second parameter against the first one when the space is of dimension two (Figure 8). On the other hand, when the curve is only characterized by one parameter, we plot the vector of the parameter against itself (Figure 7). Hence, we plot dots on a diagonal line to show where the test values lie compared to the train values. Our test set was chosen randomly but using a JAX seed to ensure reproducibility. As can be seen in the figures, we carefully chose the seeds and the number of tests to represent most of the parametric space.

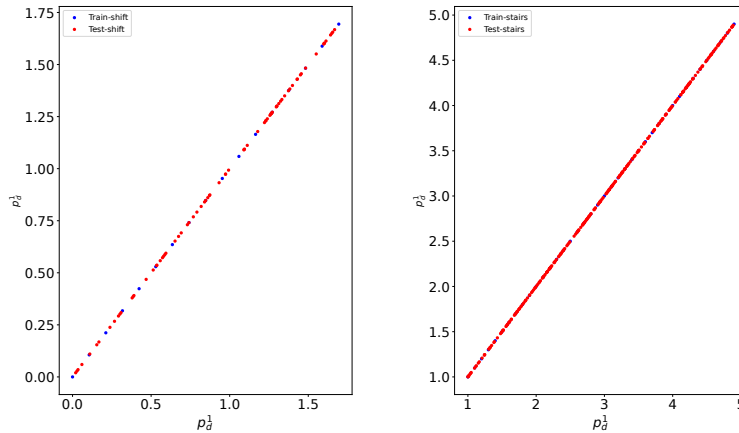


Figure 7: Train and test parameter values for the example with two shifted sine curves (left), and stair-like curves (right).

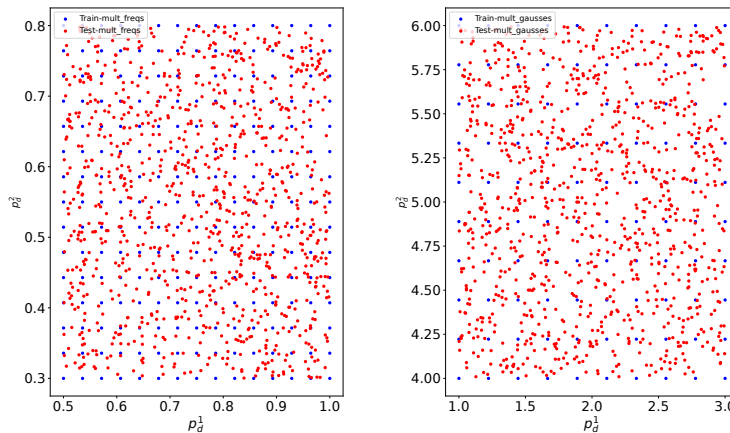


Figure 8: Train and test parameter values for the example with two accelerated sine curves (left), and two Gaussians (right).

We now explain how to exactly reproduce the test set we had. Each random parameter was created using `jax.random.uniform` which takes a `jax.random.key(seed)` as its first parameter. By choosing the same seed, the random numbers are guaranteed to be the same. Accordingly, we provide the seeds used to generate the test sets for each synthetic example in the paper. These can be found in Table 6.

Table 6: Chosen `jax.random` seeds for generating test parameters.

Problem	Shifted sine	Stairs	Two sines (freq)		Two Gaussians	
Parameter	p_d	p_d	p_d^1	p_d^2	p_d^1	p_d^2
Seed	0	0	140	8	1000	50

Appendix C Comparing RRAEs to AEs with long latent dimensions

Throughout the paper, we only compared our proposed models with others that allow feature extraction, since it is of interest to us. However, Vanilla Autoencoders with long latent spaces can interpolate very well! On both examples with the sines with two frequencies and the two Gaussians, the comparison between our strong formulation and a Vanilla Autoencoder with a latent space of dimension 2800 (same length) is shown in table 7.

Table 7: Error (in %) on our two synthetic problems for our strong formulation and an AE with the same latent dimension with no rank restriction.

Model	Mult. Freqs		Mult Gausses	
	Train Error	Test error	Train Error	Test error
AE (long)	7.96	14.08	3.37	10.56
RRAE (strong)	6.33	12.83	4.46	8.75

As can be seen in the table, reducing the rank not only allows feature extraction, it can also help in training to achieve better results and interpolation.

Appendix D Batching

In this section, we detail how batching was performed for both the weak and the strong formulations.

The weak formulation: We remind the reader that the weak formulation had the norm of $Y - UA$ in the loss, with $Y \in \mathbb{R}^{L \times D}$, $U \in \mathbb{R}^{L \times k_{max}}$, and $A \in \mathbb{R}^{k_{max} \times D}$. However, when training over batches of size bs , we have a batched latent space $Y^b \in \mathbb{R}^{L \times bs}$ and so the shape of A needs to be different. Accordingly, for each batch, we keep the indices of the vector functions used and take the column of the same indices from A to form $A^b \in \mathbb{R}^{k_{max} \times bs}$. Accordingly, for each forward/backward pass, we train different columns of matrix A .

The strong formulation: For the strong formulation, nothing changes. The truncated SVD is performed over the batched latent space $Y^b = U\Sigma V^T$. It is important to note though that since the columns change depending on the batch, the values of the right singular vector (i.e. V^T) fluctuate a lot in training. However, since the same vector U is used for all the batches, the RRAE converges towards the right basis vectors in U . After training, to be sure that training is performed over the whole dataset, we perform the truncated SVD over the entire latent space (i.e. without batching) to get the corresponding reduced basis and coefficients that are used for interpolation (i.e. the ones found in training are disregarded). Our findings are that the RRAE converges towards a unique U , which is why interpolation is so successful throughout the paper.

Appendix E Entropy as a measure of uncertainty

In section 4.2, we used the entropy to measure the uncertainty of the model. Other measures such as the Fréchet inception distance (FID) and the inception score (IS) are conventionally used/trained for colored pictures. Accordingly, we chose to use a similar concept to evaluate the generation of uncolored pictures (MNIST numbers). Using the entropy was based on IS. In general, IS is a scalar that gives an idea of how good the generated pictures are by evaluating the diversity and the quality of the generated pictures. For the IS, the entropy is a measure of the quality of the generated pictures. It is computed using the pre-trained v3 model (on colored pictures). Accordingly, we created our own version of a classifier by using a traditional CNN trained on the training set (model and training parameters found here but for 937 batches of size 64 (or one epoch), and a `softmax` instead of a `logsoftmax` with the corresponding functions modified accordingly), which predicted, from the input images, the probability of being in each class (an output in $[0, 1]^{10}$) for each architecture. By the equation of the entropy which multiplies the probability of each class by the logarithm of that probability, an ideal prediction would simply be 1 for a class and 0 for every other class (hence 100% certainty). The further the predicted values of our classifier are from 0 and 1, the harder it is to classify the pictures in the interpolated test, which means that the generated pictures don't necessarily resemble the original training set. However, we don't evaluate the diversity of the generated pictures, since our interpolation process is between two pre-specified pictures (contrary to generative models where they could generate anything).